physchem

MDPI

Article

Light-Enhanced Rechargeable Si Electrode for Li-Ion Battery with a Schottky-Type Contact as Current Collector

Oscar Vieyra-Brito [1], Estela Gómez-Barojas [1] and Enrique Quiroga-González [2,*]

[1] Research Center for Semiconductor Devices, Institute of Sciences, Benemérita Universidad Autónoma de Puebla, Puebla 72570, Mexico
[2] Institute of Physics, Benemérita Universidad Autónoma de Puebla, Puebla 72570, Mexico
* Correspondence: equiroga@ieee.org

Abstract

The present work represents a step forward in the production of a battery that can be recharged with light, without the need to integrate an energy generation device (e.g., a solar cell). Here, a silicon Li-ion battery electrode is reported, which has a current collector with an optical window that allows the impinging of light to it. The contact between the current collector and silicon is Schottky-type, behaving as a photodiode that injects charges into the electrode, which are added to the current applied to it when it is charged. The electrode presented in the present work is a proof of concept, with one of the simplest possible structures that the electrode could have to be functional (an optimized microstuctured electrode with improved charge/discharge cycling stability is envisioned): the electrode consists of monolithic silicon that has been microstructured in the backside by metal assisted chemical etching and has been decorated with Cu particles that work as a current collector. I-V curves show that the electrode by itself functions as a Schottky-type photodiode. On the other hand, when the chip is used as an electrode of a Li-ion battery, it can be properly lithiated/delithiated (it is a rechargeable electrode). Furthermore, it has been proven that when lithiation has been performed, this process has been enhanced by applying light to the current collector.

Keywords: silicon battery anode; Schottky photodiode; light-rechargeable battery; Li-ion battery; monolithic solar battery

1. Introduction

For decades, Li-ion batteries have been the subject of international research, looking to improve any characteristics of their components, particularly their charge-storing parts (the cathode and the anode). It is well known that the graphite anode of commercial batteries has a nominal storage capacity of 372 mAh/g, which has been large enough for today's batteries. However, this capacity is much smaller than the one of Si (4200 mAh/g) [1,2], which could enable lighter batteries or batteries with higher capacities. The Si-Li alloy with the highest Li content is $Li_{22}Si_5$ [3], with a Si:Li atomic proportion of 1:4.4, in contrast to the lithiation product of graphite (LiC_6) [4], with a C:Li atomic proportion of 1:0.16. However, Si has a series of drawbacks that prevent its use as an electrode of Li-ion batteries, its high volumetric expansion being the most important, because it causes fractures and capacity loss as consequence [5]. Nevertheless, this problem has been properly addressed by producing Si nanowires [6–9] and by properly charging/discharging the battery, even when the electrode has micron-sized wires or particles [4]. Then, Si-based batteries are not

Check for updates

Academic Editor: Sergei Manzhos

Received: 16 March 2026
Revised: 4 May 2026
Accepted: 3 June 2026
Published: 5 June 2026

Copyright: © 2026 by the authors. Licensee MDPI, Basel, Switzerland. This article is an open access article distributed under the terms and conditions of the Creative Commons Attribution (CC BY) license.

far from becoming a commercial reality. The same is true for Si-based electronic devices with an integrated Si-based battery.

Solar batteries (batteries that can be recharged with light) are commonly composed of a battery and a solar cell connected inside a case. Interestingly, the first solar cell, developed in 1954, was based on crystalline Si [10]. In that first solar cell, and in newer solar cell concepts, a p-n junction transforms solar light directly to electricity with relatively good conversion efficiency without applying any voltage [11,12], and the same working principle stands when using other materials [13] or other material states like polycrystal and amorphous thin films [14]. Furthermore, it is also possible to fabricate solar cells without p-n junctions, but with metal–semiconductor junctions (a Schottky-type solar cell) [15,16]. What has not been reported to date, is a battery and a solar cell monolithically coupled.

In the present work, for the first time, we have fabricated and tested a silicon Li-ion battery electrode with a current collector that makes a Schottky photodiode with Si, which injects charges into the electrode when light is applied (similar to what a solar cell does). It is a monolithic rechargeable electrode. This is a proof of concept composed of bulk Si. It is expected that the electrode presents all the long cycling stability problems of bulk Si, but they will be addressed in future work. The present work presents one of the simplest possible structures that the electrode could have to be functional.

2. Materials and Methods

The experimental route followed to obtain the microstructured Si (mSi) anode with a "transparent" Cu-Si Schottky-type contact is shown schematically in Figure 1.

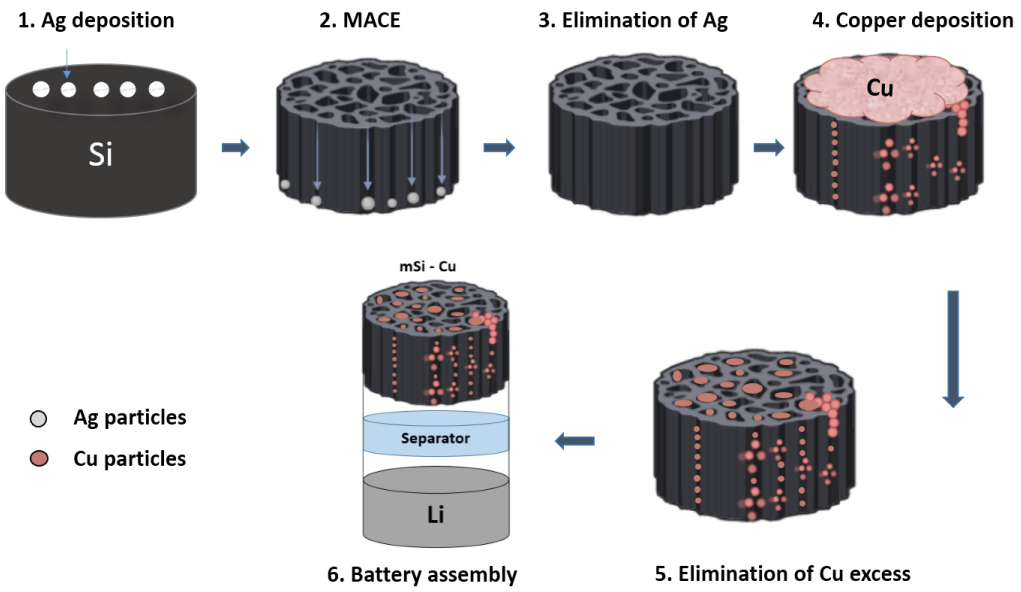


Figure 1. Schematic diagram of the fabrication of a microstructured Si-based anode for Li-ion battery with a Schottky-type contact working as photodiode.

2.1. Silicon Micro-Structuring

A p-type Si substrate 625 µm thick with (100) orientation and 15–25 Ωcm resistivity was etched by the MACE method with two steps, producing microstructured Si (mSi). In the first step, silver particles were deposited on a clean Si substrate by dipping the substrate into 10 mL of 0.01 M solution that contained 10 mL $AgNO_3$ (99%, Sigma-Aldrich, St. Louis, MO, USA) and 0.2 mL HF (48%, EMSURE, Darmstadt, Germany) according to Nagahara et al. [17].

The second step of the MACE process consisted of dipping the Ag-decorated Si substrate into an etching solution (0.01 M) that contained ($HF:H_2O_2:H_2O$) in proportion 4:1:35 $v/v/v$ at 30 °C with magnetic agitation at 300 rpm for 7 min.

2.2. Copper Deposition

Later on, Cu deposition by an electrochemical process was carried out on these mSi samples. The anodizing solution (0.01 M) was formed by 0.5 g $CuSO_4$, 133.3 mL DI water, 19.8 mL de H_2SO_4, and 33.3 mL ethanol. Then, 0.075 g of (Hexa decyltrimethyl Ammonium Bromide (CTAB) was added to this solution. The Cu deposition process was performed in an electrochemical cell; it consisted of immersing the mSi sample in the anodizing solution at 30 °C. Simultaneously, 5 mA/cm^2 current density was applied discontinuously, that is, in periods of 30 s to the anode–cathode circuit for 40 min total time, and the backside sample was illuminated continuously with a 10 W LED (λ = 680 nm) of 1 cm^2 in order to improve Cu deposition [18]. The final product is called mSi-Cu in this work.

2.3. Structural Characterization

The final structures were analyzed with a JEOL JSM-7500F (JEOL Ltd., Tokyo, Japan) field emission scanning electron microscope (FE-SEM), which is equipped with an X-Max (Oxford Instruments, Buckinghamshire, UK) Energy Dispersive X ray spectrometer (EDX) detector to perform elemental analysis.

2.4. Electrical and Electrochemical Characterization

Current–voltage (I-V) measurements were performed on mSi-Cu by placing a probe on the Cu side and one contact on the back, using a 4200-SCS semiconductor analyzer from Keithley (Solon, OH, USA). Measurements were performed in the voltage range of −6 to 6 V at a 0.02 V/s rate under darkness and under illumination. The sample was illuminated with a 10 W LED (λ = 680 nm) with efficiency of about 100 lm/W and an active area of 1 cm^2. This light source was set at a distance of 5 cm, representing a luminance of 6.37×10^4 lx.

The anodes were assembled in half battery cells with metallic Li as counter electrode and a Whatman filter paper as a separator. The electrolyte was a solution 1 M of $LiPF_6$ in ethylene carbonate and dimethyl carbonate in a proportion 50:50 v/v. Charge/discharge cycling tests were performed with an MTI (Richmond, CA, USA) battery cycler in galvanostatic mode by applying a current density of 0.02 mA/cm^2 and taking 0.02 V and 1.5 V as the voltage limits. Cyclic voltammetry in selected small voltage ranges was performed in a ZENNIUM potentiostat of Zahner (Kronach, Germany) at a voltage sweep rate of 0.2 mV/s under darkness and under illumination. The sample was illuminated under the same conditions described in the previous paragraph.

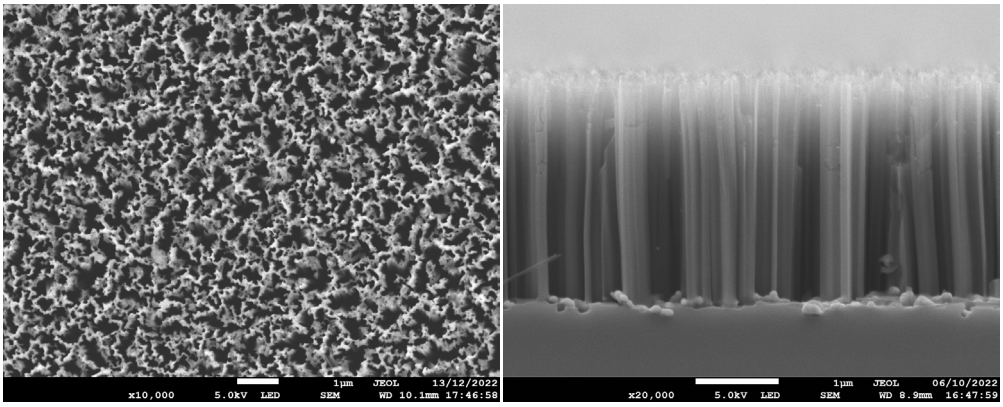
3. Results and Discussion

3.1. Structural and Compositional Characterization

Figure 2 shows SEM micrographs in which the micro-structure of the Si substrate can be observed after it has been etched by the MACE method. In (a), at 10,000 magnification (×), it is observed that the surface morphology is formed by pores delimited by nanowalls (<100 nm). In (b), at 20,000×, the area shows parallel macropores of about 3 μm in length.

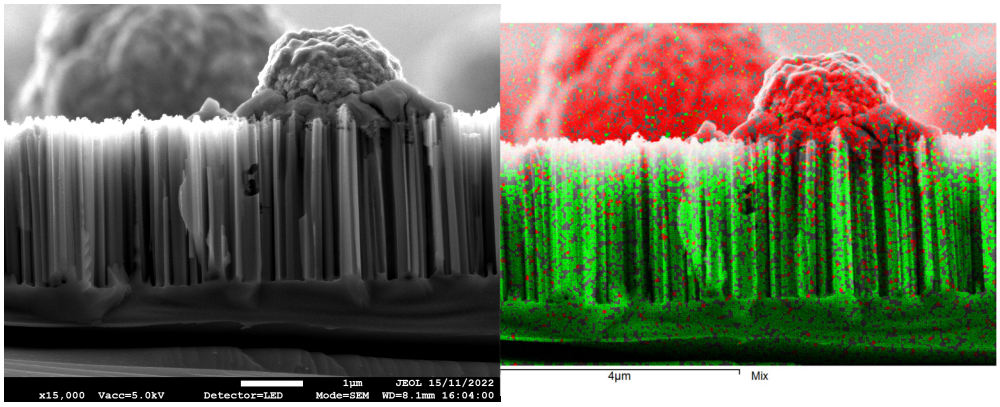
Furthermore, according to the EDS mapping shown in Figure 3, small Cu (in red) particles are positioned on the micropore walls, and on the top surface, the Cu particles are greatly agglomerated.

Later on, Cu deposition by an electrochemical process was optimized by adding 5 times the amount of CTAB (0.375 g) to the anodizing solution, the current density was applied continuously for 20 min, and the backside of the sample was continuously illuminated with an LED (λ = 680 nm). The result of the plating solution optimization for the electrochemical Cu deposition process can be observed in Figure 4, where it is seen that the Cu particles are deposited aleatorily on the pore walls and on the bottom with greater density.



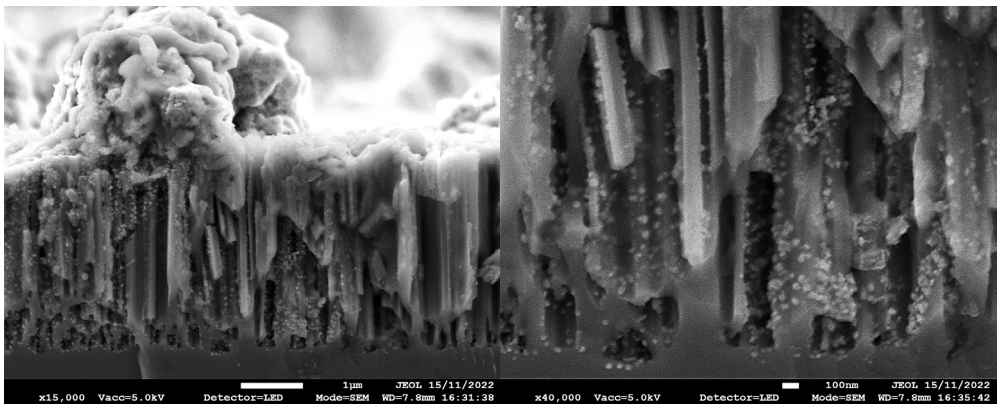
(**a**) (**b**)

Figure 2. SEM micrographs of Si etched by MACE: (**a**) surface morphology and (**b**) cross-section view.



(**a**) (**b**)

Figure 3. (**a**) SEM micrograph of a cross-section of an mSi with Cu deposition and (**b**) an EDS mapping. The green color denotes Si and the red color marks Cu distribution.



(**a**) (**b**)

Figure 4. Cross-section SEM micrographs of an mSi sample with Cu particles on the pores walls: (**a**) at 15,000× showing the complete structure evidencing Cu agglomerates of about 3.5 µm in diameter on the surface, and (**b**) at 40,000× evidencing the Cu nanoparticles decorating the pore walls.

Figure 4 shows cross-section view SEM micrographs of mSi with Cu deposits. In (a), at 15,000×, we observe Cu particles deposited on the pore walls; also, on the uppermost surface of the mSi sample, a huge agglomeration is observed. In (b), a micrograph at 40,000× shows the particles are deposited aleatorily on pore walls and on the bottom.

3.2. Test of the Device as a Photodiode

The I-V curves of the mSi-Cu sample are shown in Figure 5. In (a), we observe a full voltage range plot, indicating a rectifying diode behavior: it conducts under direct polarization (negative voltage range in the present device), and it practically does not conduct under inverse polarization (positive voltage range). The inverse current is 3 orders of magnitude smaller. Particularly, it behaves as a Schottky diode, considering that is based on a metal–semiconductor junction. In this figure, an increase in current is also evident when light is impinged on the sample, due to the photocurrent (it works as a photodiode).

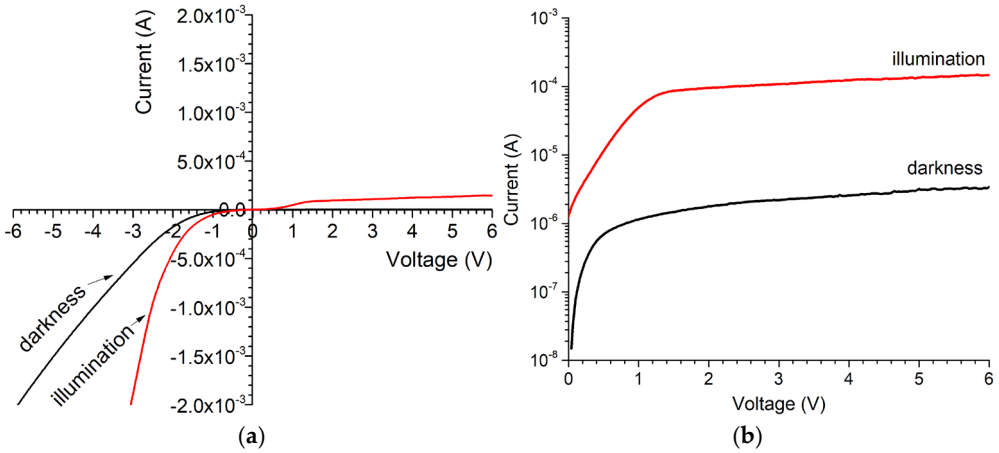


Figure 5. I-V plots of the mSi-Cu sample: (**a**) full range from −6 to 6 V, exhibiting a typical rectifying diode behavior. (**b**) Close-up in the range of 0 to 6 V, allowing us to see the difference of 2 orders of magnitude between the response under illumination and darkness.

In a close-up of the range of inverse polarization (Figure 5b), it is possible to observe an increase of 2 orders of magnitude in the current when light is impinged on the sample. This means a signal-to-noise ratio of 100, which is competitive for photodetectors.

Interestingly, the I-V curve obtained under direct polarization cannot be fitted with the typical equation of the current I of a Schottky barrier:

$$I = I_s\left(e^{\frac{qV}{nKT}} - 1\right) \quad (1)$$

where I_s is the saturation current, q is the charge of the electron, n is an ideality factor, K is the Bolzman constant, V is the applied voltage, and T is the temperature in Kelvin.

The increase in current is not exponential, but quadratic at low voltages, as when Fowler–Nordheim (F-N) tunneling occurs:

$$I = AV^2\left(e^{-\frac{B}{V}}\right) \quad (2)$$

where A and B are constants that depend on physical parameters of the junction.

The result of the fitting is shown in Figure 6, plotting $\ln(I/V^2)$ vs. $1/V$. As expected, the resulting curves for the current under darkness and under illumination are straight lines.

It is quite surprising that the current behaves like Fower–Nordheim (F-N) tunneling, which commonly occurs at high voltages, at which the barriers are triangular. It is the dominant transport mechanism at low voltages, although a Schottky-type junction may be present. In the present case, tunneling is obtained at low voltages (the threshold voltage is about 0.6 V for both cases, darkness and illumination). This means that the width of the barrier should be very thin. The surface of porous silicon, where Cu is deposited, should have a thin SiO_2 layer, naturally grown on Si (native oxide). This behavior has been previously observed, but in so-planned metal–insulator–semiconductor (MIS) structures of Ag-Al_2O_3-ZnO [19]. When Al_2O_3 was eliminated, it was also possible to observe F-N

tunneling, but it originated from the charge transport between ZnO wires and not because of the transport through the metal–semiconductor junction. Another possibility is that the metal–semiconductor barrier of the present case is very thin because of the presence of an excess of carriers due to the defect-rich porous Si surface.

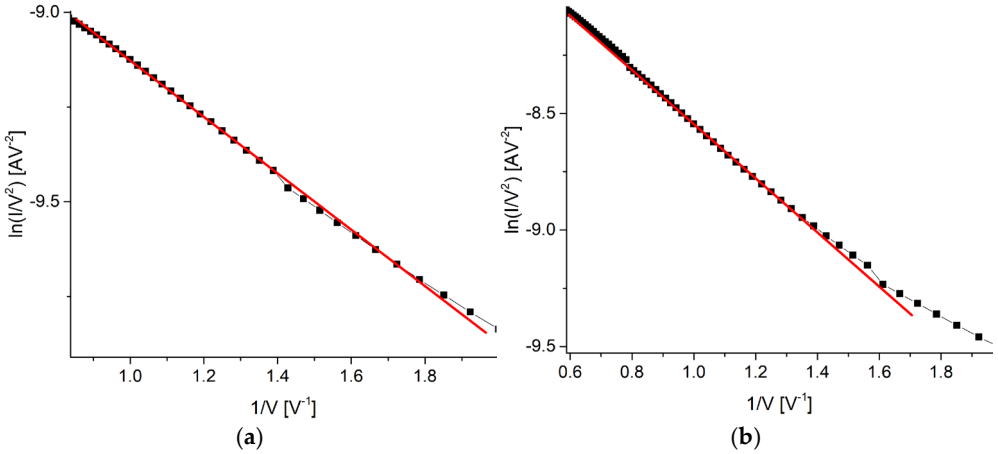


Figure 6. ln(I/V^2) vs. 1/V plots to denote Fowler–Nordheim tunneling: (**a**) under darkness; (**b**) under illumination.

Figure 7 shows an I-V curve of the mSi-Cu when light was applied during a reverse voltage sweep in an intermittent way at a pace of 87 mHz with a 60% "on" period. The response is around 0.5 s (it is not resolved exactly, due to the limitation in the number of data points, as can be observed in the inset). This time mainly depends on the shutter, which moved at a linear pace.

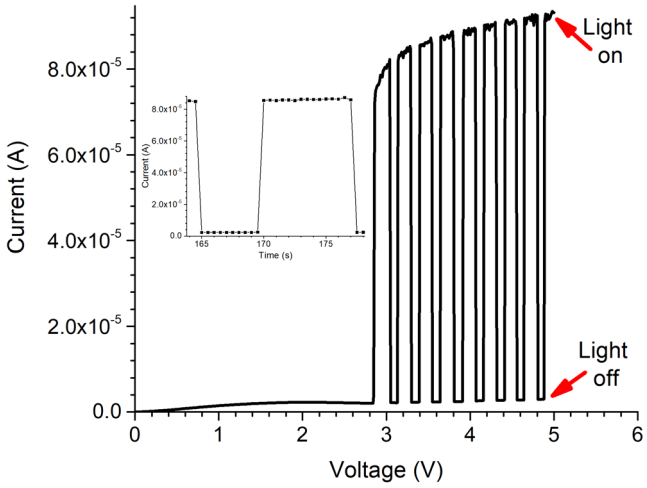


Figure 7. I-V plot of the mSi-Cu sample under switching conditions of darkness and illumination. The inset is a close-up of one switching cycle.

3.3. Test of the Device as a Battery

Figure 8 shows a voltage vs. capacity curve measured during the ninth lithiation/delithiation cycle; the maximum lithiation capacity (100%) was reached (see Figure S1 of the Supplementary Materials). The delayed stabilization occurs because of the large thickness of the electrode (the full capacity can just be reached after multiple cycles because the capacity is limited by voltage during the galvanostatic cycling). On the other hand, an excess of charges is used during the first cycles by the electrode to form the solid electrolyte interphase (SEI), as is common in Si-based electrodes [20]. After the ninth cycle, the capacity

drops dramatically, as can be seen in Figure S1, probably due to electrode cracking, since bulk Si was used for the present proof of concept. This problem will be addressed in future work, when the performance will be in focus.

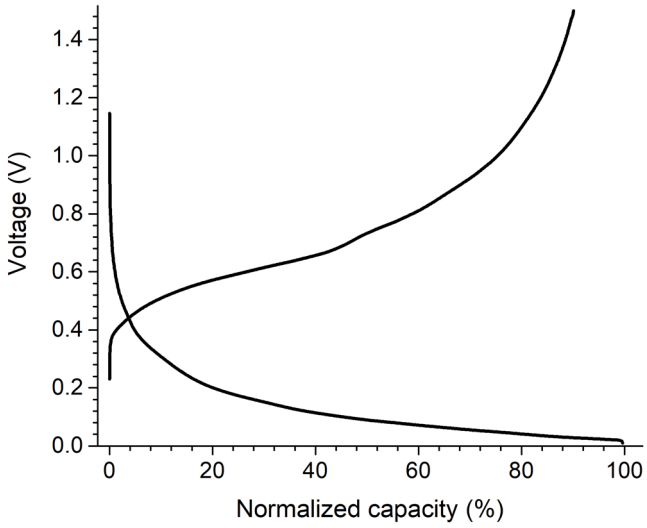


Figure 8. Voltage vs. normalized capacity of a lithium ion battery half cell with mSi-Cu working electrode during cycle 9.

Cyclic voltammetry is a technique useful to identify either redox processes or change in phase processes that imply charges in an electrochemical storage system [2,4,21]. However, as bulk Si lithiates slowly potentiostatically, no clear peaks are observed by this technique in the present electrodes, even performing the experiment at rates as slow as 0.02 mV/s. That is why, instead of this technique, we have used an analogous one, which consists of calculating the first derivative of voltage vs. capacity curves (obtained galvanostatically), with a procedure indicated in the Section 2. The resulting curves are shown in Figure 9. This is a procedure previously used in our group to denote processes occurring in Si electrodes, with remarcable results to characterize the electrodes in situ while being charged–discharged [20].

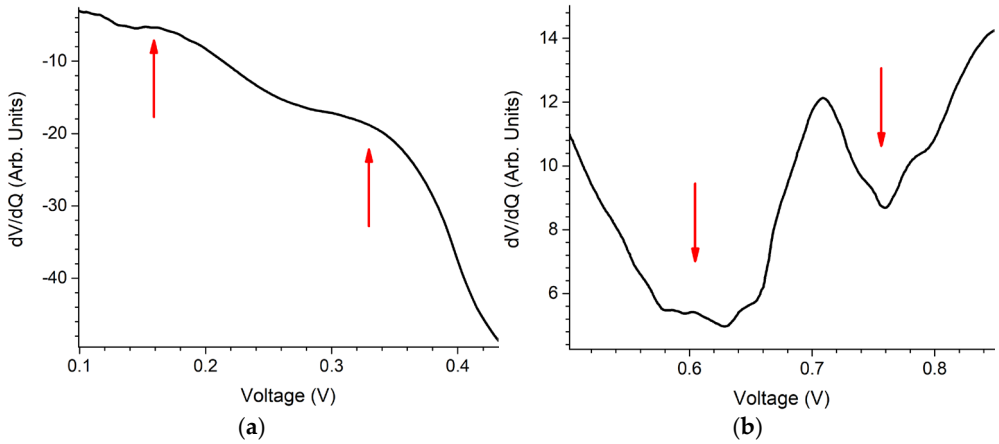


Figure 9. dV/dQ vs. voltage curves of cycle 9 (Figure 7) for (**a**) lithiation, (**b**) delithiation.

As can be observed, two peaks pointing up (at around 0.15 and 0.33 V) are obtained for the lithiation curve, and two peaks pointing down (at around 0.6 and 0.75 V) are obtained for the delithiation curve. The position of the peaks differ for about 150 mV with respect to the ones reported in the literature [2,4]. This is due to Ohmic drops, probably because

the current collector is not a continuous Cu plate but Cu nanoparticles decorating the microstructured Si or because of the increase in impedance of the Si electrode upon cycling, as commonly occurs even in microestructured electrodes due to expansion/contraction and amorphization [20], until a mechanical quasi-stationary state is reached. However, it is shown that the same number of electrochemical events for the insertion and extraction of lithium in/from Si occur as reported in the literature, proving that the developed electrode functions as other Si-based electrodes with no additional reactions [2,4].

3.4. Proof of Concept: Light-Enhanced Rechargeable Monolithic Si Electrode for Li-Ion Battery

Figure 10 shows I-V curves of a lithium ion battery half cell with mSi-Cu working electrode; (a) was obtained applying a negative voltage sweep in the 0.19–0.15 V range, around the voltage range of a Si lithiation event, and (b) was obtained applying a possitive voltage sweep in the 0.5–0.53 V range, close to the uptake position of the first delithiation peak of Figure 9. An increasing negative current lithiates Si, and an increasing positive current delithiates Si. In both curves, the currents are negative due to leakage current in the battery assembly, which does not prevent the device from performing as a battery.

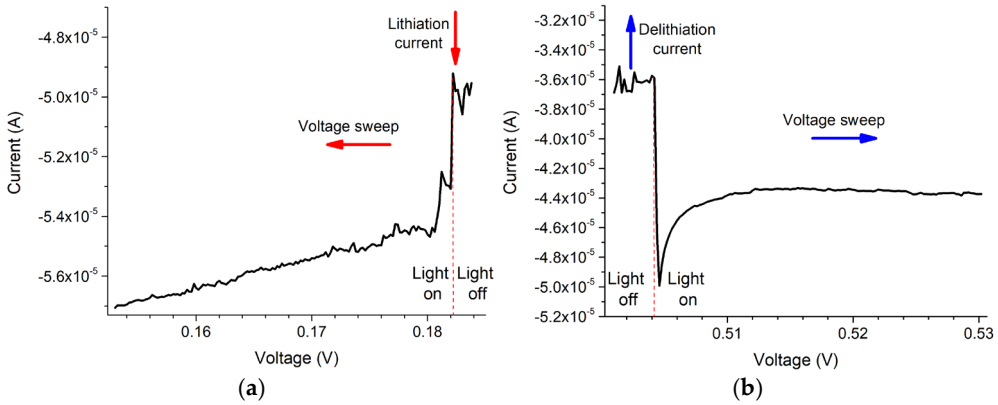


Figure 10. Voltammetry tests in selected small voltage ranges of a lithium ion battery half cell with mSi-Cu working electrode, illuminatied at the back side after a short time under darkness: (**a**) negative voltage sweep for lithiation, and (**b**) possitive voltage sweep for delithiation.

More importantly, as can be observed, when light is impinged at the backside of the Si electrode, the current goes to more negative values independently of the voltage sweep direction. This means that the electrode lithiates when light is applied. In a full battery, when the Si-based electrode is used as anode, the lithiation of Si occurs when the battery is being charged; then, we can infer that, if an mSi-Cu electrode is used as an anode and light is applied at its backside, the battery charging process is enhanced.

4. Conclusions

We successfully fabricated and tested a Li-ion battery electrode that has the additional function of enhancing the charging process with light. It consists of monolithic Si that has been microstructured at the backside, where Cu is electrochemically deposited to be used as a current collector and as a Schottky-type photodiode.

I-V curves of the electrode outside a battery show that it behaves like a photodiode. Nevertheless, the charge transport is dominated by Fowler–Nordheim tunneling at low voltages. Noteworthy is that, when the electrode is inversely polarized, the difference in current response is of two orders of magnitude larger when light is applied. On the other hand, it could be switched with light at a rate of 87 mHz, just limited by the shutter used.

When the electrode is assembled in a Li-ion battery, it exhibits the typical electrochemical processes occurring in Si electrodes. It does not have the best performance because

it is made of bulk Si (it is slow to be lithiated/delithiated and could be broken after prolonged cycling). However, it is the simplest proof of concept, which could be improved by micromachining, as achieved in previous works by our group.

Finally, it has been proven that the monolithically grown Schottky-type photodiode serves to enhance the electrode lithiation when applying light. This effect could represent charging enhancement in Li-ion batteries using the here-developed electrode as an anode.

Supplementary Materials: The following supporting information can be downloaded at https://www.mdpi.com/article/10.3390/physchem6020033/s1, Figure S1: Capacity and coulombic efficiency curves of the mSi-Cu electrode in a Li-ion battery half cell.

Author Contributions: O.V.-B.: formal analysis, investigation, writing—original draft preparation, data curation; E.G.-B.: investigation, writing—original draft preparation; E.Q.-G.: writing—review and editing, methodology, formal analysis, resources, project administration, funding acquisition, supervision. All authors have read and agreed to the published version of the manuscript.

Funding: This research was funded by Secretaría de Ciencia, Humanidades, Tecnología e Innovación (SECIHTI) through the project CBF-2025-I-2794.

Institutional Review Board Statement: Not applicable.

Data Availability Statement: The original contributions presented in this study are included in the article/Supplementary Materials. Further inquiries can be directed to the corresponding author.

Acknowledgments: O. Vieyra-Brito thanks the SECIHTI for a scholarship grant.

Conflicts of Interest: The authors declare no conflicts of interest.

References

1. Teki, R.; Datta, M.; Krishnan, R.; Parker, T.; Lu, T.; Kumta, P.; Koratkar, N. Nanostructured silicon anodes for lithium ion rechargeable batteries. *Small J.* **2009**, *20*, 2236–2242. [CrossRef] [PubMed]
2. Quiroga-González, E.; Carstensen, J.; Föll, H. Good cycling performance of high density arrays of Silicon microwires as anodes for Li ion batteries. *Electrochim. Acta* **2013**, *101*, 93–98. [CrossRef]
3. Okamoto, H. Li-Si (Lithium-Silicon). *J. Phase Equilibria Diffus.* **2009**, *30*, 118–119. [CrossRef]
4. Quiroga-González, E.; Ossei-Wusu, E.; Carstensen, J.; Föll, H. How to Make Optimized Arrays of Si Wires Suitable as Superior Anode for Li-Ion Batteries. *J. Electrochem. Soc.* **2011**, *158*, E119–E123. [CrossRef]
5. Li, J.-Y.; Xu, Q.; Li, G.; Yin, Y.-X.; Wan, L.-J.; Guo, Y.-G. Research progress of Si-based anode materials to-wards practical application in high energy density Li-ion batteries. *Mater. Chem. Front.* **2016**, *1*, 1691–1708. [CrossRef]
6. Aca-López, V.; Quiroga-González, E.; Gómez-Barojas, E.; Swiatowska, J.; Luna-López, J.A. Effects of the doping level in the production of silicon nanowalls by metal assisted chemical etching. *Mater. Sci. Semicond. Process.* **2020**, *118*, 105206–105213. [CrossRef]
7. Pérez-Díaz, O.; Quiroga-González, E.; Hansen, S.; Silva-González, N.R.; Carstensen, J.; Adelung, R. Fabrication of silicon microwires by a combination of chemical etching steps and their analysis as anode material in Li-ion batteries. *Mater. Technol.* **2019**, *34*, 785–791. [CrossRef]
8. Ma, D.; Cao, Z.; Hu, A. Si-Based Anode Materials for Li-Ion Batteries: A Mini Review. *J. Nano-Micro Lett.* **2014**, *6*, 347–358. [CrossRef] [PubMed]
9. Liu, Y.; Ji, G.; Wang, J.; Liang, X.; Zuo, Z.; Shi, Y. Fabrication and photocatalytic properties of silicon nanowires by metal-assisted chemical etching: Effect of H_2O_2 concentration. *Nanoscale Res. Lett.* **2012**, *7*, 663. [CrossRef] [PubMed]
10. Chapin, D.M.; Fuller, C.S.; Pearson, G.L. A new p-n Junction Photocell for converting solar radiation into Electrical Power. *J. Appl. Phys.* **1954**, *25*, 676. [CrossRef]
11. Streetman, B.G.; Banerjee, S.K. *Solid State Electronic Devices*, 6th ed.; Prentice Hall: Hoboken, NJ, USA, 2000.
12. Neamen, D.A.; Biswas, D. (Eds.) *Semiconductor Physics and Devices: Basic Principles*, 4th ed.; McGraw-Hill: New York, NY, USA, 2011.
13. Raynolds, D.C.; Leies, G.; Antes, L.L.; Marburger, R.E. Photovoltaic Effect in Cadmium Sulphide. *Phys. Rev.* **1954**, *96*, 533. [CrossRef]
14. Sze, M. *Physics of Semiconductor Devices*, 2nd ed.; John Wiley and Sons: New York, NY, USA, 2008.
15. Le Duc, T.; Moyen, E.; Zamfir, M.R.; Joe, J.; Yan, X.; Zhang, Y.; Pribat, D. New Schottky-Type Wire-Based Solar Cell with $NiSi_x$ Nanowire Contacts. *ACS Appl. Mater. Interfaces* **2020**, *12*, 37464–37469. [CrossRef] [PubMed]

16. Chowdhury, K.; Mandal, R. Advancement of Schottky barrier solar cells: A review. *Top. Intell. Comput. Ind. Des. (ICID)* **2020**, *2*, 93–98.
17. Nagahara, L.A.; Ohmori, T.; Hashimoto, K.; Fujishima, A. Effects of HF solution in electroless deposition process. *J. Vac. Sci. Technol.* **1993**, *11*, 763–767. [CrossRef]
18. Tobail, O.; Quiroga-González, E.; Carstensen, J.; Föll, H. Enhancement of Cu Filling into p-Type Macro-Porous Silicon by Pore Wall Thinning, Oxide Deposition and Back Side Illumination. *J. Electrochem. Soc.* **2014**, *161*, D657–D662. [CrossRef]
19. Bayan, S.; Mohanta, D. Significant Fowler-Nordheim tunneling across ZnO—Nanorod based nanojunctions for nanoelectronic device applications. *Curr. Appl. Phys.* **2013**, *13*, 705–709. [CrossRef]
20. Quiroga-González, E.; Carstensen, J.; Föll, H. Structural and electrochemical investigation during the first charging cycles of silicon microwire array anodes for high capacity lithium ion batteries. *Materials* **2013**, *6*, 626–636. [CrossRef] [PubMed]
21. Evans, D.H.; O'Connell, K.M.; Petersen, R.A.; Kelly, M.J. Cyclic voltammetry. *J. Chem. Educ.* **1983**, *60*, 290. [CrossRef]

Disclaimer/Publisher's Note: The statements, opinions and data contained in all publications are solely those of the individual author(s) and contributor(s) and not of MDPI and/or the editor(s). MDPI and/or the editor(s) disclaim responsibility for any injury to people or property resulting from any ideas, methods, instructions or products referred to in the content.